

Powder Metallurgical Fabrication and Characterization of Nanostructured Porous NiTi Shape-Memory Alloy

S. K. SADRNEZHAAD, H. ARAMI, H. KEIVAN, AND R. KHALIFEZADEH

Department of Materials Science and Engineering, Center of Excellence for Advanced Processes of Production and Shaping of Materials, Sharif University of Technology, Tehran, Iran

Production of NiTi alloy from elemental powders was conducted by mechanical alloying (MA) and sintering of the raw materials. Effects of milling time and milling speed (RPM) on crystallite size, lattice strain, and XRD peak intensities were investigated by X-ray analysis of the alloy. Powder compaction and sintering time and temperature effects on pore percentage of the as-mixed and the mechanically alloyed samples were empirically evaluated. The crystallite size of the mechanically alloyed Ni₅₀Ti₅₀ samples decreased with MA duration and with the milling speed. Depending on the crystal structure of the raw materials, the lattice strain increases with the milling duration. Metallographic studies proved the existence of martensitic B19' after sintering of both the as-mixed and the mechanically alloyed samples. Its amount was, however, greater for the former. Sintering lowered the porosity of the samples; no matter what powder (as-mixed or mechanically alloyed) was used. The porosity was greater, however, for the MA powders. This difference seemed to be due to the sharper liquid phase sintering effect of the as-mixed samples.

Keywords Lattice strain; Mechanical alloying; Nanostructure; NiTi; Powder metallurgy; Sintering; SMA.

INTRODUCTION

NiTi shape-memory alloy (SMA) has excellent sensing–actuating properties. Acceptable biocompatibility [1, 2], good corrosion resistance [3, 4] and promising osteointegration potential [5] have been reported especially for NiTi porous alloys. Highly crystalline ultra-pure nanoparticles produced by mechanical alloying–combustion synthesis (MA–CS) provide very high surface area desirable for better osteogenic properties. The application of innovative nanotechnology can improve success rate of implants for orthopedic and dental applications. Nanocrystalline NiTi implants are of special interest because of their high atomic concentration in interfacial structures, desirable mechanical properties and relatively simple way of production [6].

An important feature of NiTi is its delicate response to a temperature change or a mechanical force [8, 9]. The former is due to the one-step phase transformation of B2 to B19' [10, 11]. The latter is due to the stress-induced austenite to martensite (A–M) phase transformation [11]. Temperature-dependent first-order displacive (martensitic) transformation of higher-symmetry cubic crystals to lower-symmetry rhombohedral, tetragonal, orthorhombic or monoclinic phase results in coupled thermomechanical shape memory behavior in NiTi alloys [12]. Superelastic response of porous NiTi samples has been modeled by different authors [12, 13]. Previous researchers have proposed nanomechanical atomic potential models to find the role of temperature on perfect crystal equilibrium path in a

stress-free bi-atomic alloy system [7, 12]. Rapid strain variation across the A–M interface has been reported in the nanosized NiTi grains [6, 14].

Information on production and property characterization of NiTi nanoparticles is very limited. Traditional vacuum induction melting (VIM) accompanied with casting has been used for production of NiTi objects [15]. Nonequilibrium intermetallic phase formation and high levels of oxide, nitride and carbide impurities embedded within the phases have been the matter of much concern [16, 17]. Many investigations have focused on combustion synthesis (CS) also called self-propagating high temperature synthesis (SHS) or powder metallurgy (PM) for production of bulk NiTi phase [20–24]. Significant interest exists in liquid-phase sintering [26]. Large dimensional change and low packing density after sintering are two undesirable drawbacks that should somehow be remedied. Fixtured sintering is proposed as a means of reducing the dimensional change of the sintered NiTi objects [26].

NiTi nanocrystalline powders can be produced in a number of ways. Electro-explosion of NiTi wire results in dispersion of very small aerosol particles from cold argon atmosphere [27]. Shock synthesis of the mechanically amorphized NiTi powder followed by crystallization heat treatment is reported to increase the martensitic start transformation temperature [28]. Sintering of very fine TiH₂ with Ni powder is used to produce Ti-rich NiTi alloy. Results show that fine porosity forms from the use of TiH₂ powder [29]. High-speed deformation processing can also result in local nonequilibrium nanophase formation [18]. Modulated structural bands consist of numerous nanophase domains [18]. Various local nonequilibrium nanophases formed due to high-speed deformation appear to be R-phase (Ni₄Ti₃ with some vacancies), O-phase (Ni₃Ti₂), and amorphous NiTi phase [18, 19]. Various phase transitions appear to be signaled by nano-band crossing effects. Metastable phases are observed frequently in such locations [18].

Received May 20, 2005; Accepted August 1, 2005

Address correspondence to S. K. Sadrnezhad, Department of Materials Science and Engineering, Center of Excellence for Advanced Processes of Production and Shaping of Materials, Sharif University of Technology, P.O. Box 11365-9466, Tehran, Iran; Fax: +9821-66005717; E-mail: sadrnezh@sharif.edu

Research on processing of nanomaterials into bulk objects with engineered properties for manufacturing of new devices and procedures is of much interest to engineers. The main objective of this investigation is production of a newly made homogeneous material with a controlled porosity percentage and an extreme grain refinement before subsequent consolidation by a compaction/sintering operation [32]. Porosity, density, and crystallite size changes during vacuum sintering of the ground powders are empirically investigated and theoretically explained. Effect of mechanical alloying–sintering conditions on NiTi porosity and nanocrystallite formation is discussed in detail.

Two sets of as-mixed and milled samples are thoroughly compared. Most recent investigations carried out on effects of time, temperature and milling rate on physico-chemical properties of the NiTi powders prepared for manufacturing sintered objects are reported. The work aims to obtain a fundamental understanding of the material behavior during powder metallurgical fabrication of nanostructured porous NiTi shape-memory alloy as a potential candidate for utilization in micro-electromechanical systems (MEMS), micropumps, microwrappers and stents for neurovascular blood vessels. Research on nano-electromechanical systems (NEMS), nanowires (NW), and nanoparticles (NP) are certainly of potential interest for numerous future applications.

Porous NiTi has newly been introduced as a biomaterial with great applications [25]. Porosity is believed to help osteointegration [5]. Its higher specific surface may, however, increase the rate of corrosion. Nanocrystal formation improves mechanical specifications. How to control the porosity fraction is not described in the literature. Recovery rate depends on this parameter, however. Effect of milling time and sintering conditions on porosity percentage and crystallite size are desirable outcomes of this investigation. Best osteointegration, least corrosion rate, greatest mechanical strength and highest healing speed are further goals of the research.

EXPERIMENTAL PROCEDURE

Commercially pure elemental powders of titanium and nickel—both from Merck Inc. of Germany—were blended at room temperature in a ball attritor mill made of polyamide compound for up to 20 hours. The milling speeds were 350, 600, and 750 rpm. Initial mean particle size of both powders was 30–40 μm . The polyamide container was charged with 20 g of a titanium/nickel equiatomic powder mixture initially and 200 g of hardened steel balls with different diameters averaging 5 mm. The ball-to-powder charge ratio was 10:1. The process was performed under argon atmosphere.

Milling periods of 20 min were alternated with equal resting times in order to avoid the temperature increase during milling. The milling was interrupted at regular intervals to collect a small amount of powder for phase analysis using X-ray diffraction (XRD) with Cu-K_α and Co-K_α radiation in a PW1390 Philips machine (Eindhoven, The Netherlands).

Cylindrical pills (1.5 cm diameter and around 0.2 cm thickness) of mechanically alloyed powders were

compacted under 400, 500, and 600 MPa pressure. The pills were placed inside a carefully machined fixture made of DIN 1.4821 heat-resistant steel similar to the one described in Sadreznhaad and Lashkari [26] and heated in a vacuum resistance furnace for different temperatures and different periods of time. The furnace had first been purged with pure argon and then evacuated to a vacuum of 10 mm Hg or lower.

The pills were polished and then etched in a solution containing 75 vol.% H_2O , 15 vol.% HNO_3 and 10 vol.% HF. An Olympus optical microscope was used to observe the microstructure of the specimens. Densities of the heat treated samples were measured with a Sartorius-CP324S densitometer (Bradford, MA, USA).

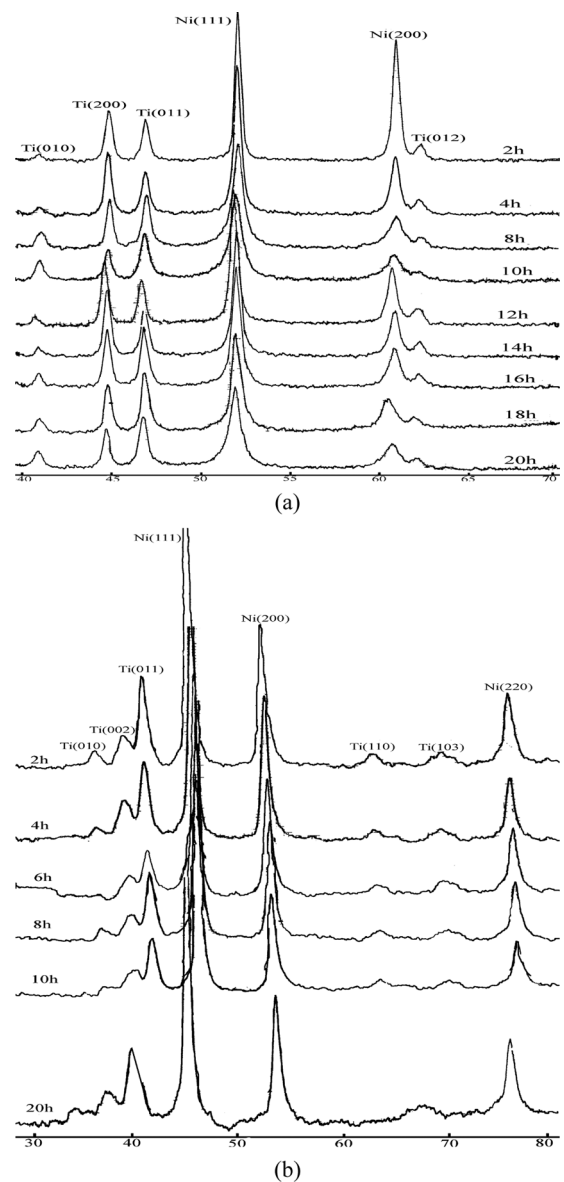


FIGURE 1.—X-ray diffraction spectra of mechanically alloyed powders after different milling times: (a) Co-K_α , 350 rpm and (b) Cu-K_α , 600 rpm.

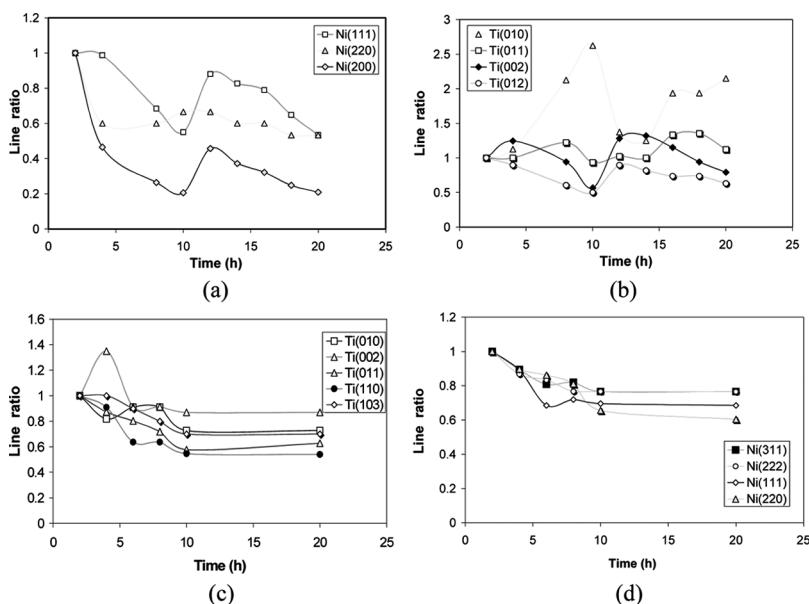


FIGURE 2.—X-ray line ratios of Ti and Ni for different planes as a function of milling time at different milling speeds of: (a and b) 350rpm with Co-K α and (c and d) 600rpm with Cu-K α .

RESULTS AND DISCUSSION

Phase identification was performed both before and after sintering using XRD plots of the samples milled for different periods of time. Typical X-ray spectra obtained at milling speeds of 350 and 600rpm are shown in Fig. 1. Effect of milling time on the XRD line intensity ratios of different Ti and Ni planes is shown in Fig. 2. It can be seen that the corresponding intensity lines of the nickel high density FCC planes—i.e., (111), (200), and (220)—and the titanium high density HCP planes—i.e., (103), (012), (011), (002), and (010)—widen and weaken as a result of the powder milling process. The reason for these changes will be discussed later.

Williamson–Hall XRD line-broadening analysis [25, 33] was performed to determine the average crystallite size and lattice strain of the Ni and Ti elements at different milling times and speeds. The values of $B\cos\theta$ were plotted against $\sin\theta$, in which B is the line width (in radians) at the half maximum intensity of the peak, and θ is the Bragg diffraction angle. The slope of the straight line passing through the experimental data is equal to the lattice strain. The intercept of the line is equal to $(0.9\lambda)/d$, in which λ is the wavelength of the X-ray used and d is the crystallite size. Figures 3 and 4 show the Williamson–Hall plot of Ni and Ti powders at different milling times and rotational speeds, respectively.

The lattice strains of both nickel and titanium evaluated by the above-mentioned method are shown in Fig. 5. Experimental data show that the lattice distortion of both nickel and titanium increases with the milling time and speed. After 20 hours of milling, the mean distortion values for Ni are 1.32%, 1.5%, and 1.62% and for Ti are 1.62, 4.1, and 4.9%, corresponding to the milling speeds of 350, 600 and 750 rpm, respectively.

Milling also causes refinement of the crystallites. This phenomenon is simply observable from the data given in

Fig. 6. The crystallite size decreases with increasing lattice strain. Effects of milling time and milling speed on lattice strain and crystallite size are demonstrated in Fig. 7.

Both elastic energy and structural instability of the Ni–Ti alloy were increased with the lattice strain. These parameters could be used to explain the increasing free energy, the lattice disordering and the subsequent formation of the amorphous phase with mechanical alloying of the mixed powder. Disorder and nanocrystalline grain boundaries may increase the free energy and therefore act as driving force for the order-to-disorder and crystallite-to-amorphous transition. The crystallite sizes of nickel and titanium powders decrease drastically from the initial sizes to about 23.9 and 22.01 nm after 20h of milling at rotational speed of 750 rpm.

XRD spectra of samples milled for different rotational speeds are shown in Fig. 8. With a higher milling speed, both nickel and titanium peaks become broader and weaker. X-ray line ratios of the different planes are shown in Fig. 9 for Ti and Ni as a function of the speed of rotation. An increase in the milling speed shifts both nickel and titanium peaks slightly towards lower angles (see Fig. 10). This means that the lattice parameters of the FCC nickel and HCP titanium increase with increasing of speed of rotation. The variation of the lattice parameters (a_0) of nickel and titanium crystals is displayed as a function of the speed of rotation in Fig. 11. The faster the milling rotational speed, the higher the energy input into the powders. The mean lattice strain increases and the average nanocrystal size decreases with the milling rate.

Figure 11 shows that the lattice parameter (a_0) monotonically increases with the milling speed. Increasing RPM enhances the solid-state reaction so that the Ti atoms begin to migrate to the Ni lattice sites. This leads to a monotonic expansion in the value of a_0 for pure Ni to form a solid solution (Fig. 11). The increase in the nickel lattice

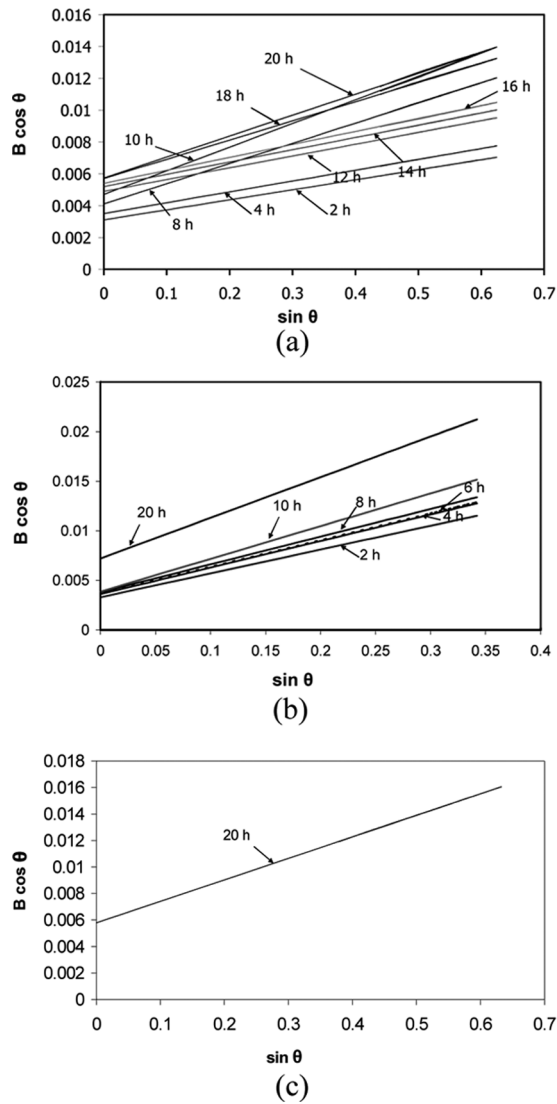


FIGURE 3.—Effect of milling time on Williamson–Hall plot [24] of Ni powders milled at (a) 350rpm characterized by Co- K_{α} , (b) 600rpm characterized by Co- K_{α} , and (c) milled for 20 hours at 750rpm characterized by Cu- K_{α} .

parameter indicates that the titanium atoms, which have a smaller atomic radius than nickel atoms, dissolve into FCC nickel and form a disordered face centered cubic (FCC) solid solution of titanium in nickel. A metastable amorphous phase is thus produced after an appropriate mechanical alloying treatment.

Fixtured sintering decreased porosity and increased density of the samples. Figure 12 compares the morphology of the mixed–pressed–sintered specimens with that of the milled–pressed–sintered ones. Martensitic B19' blades are clearly seen in the surface images of the sintered samples [Figs. 12(c) and (d)], no matter from what initial powder they are made [compare Fig. 12(c) with Fig. 12(d)]. The B19' percentage is, however, greater for the samples made of the as-mixed powders. This seems to be due to the sharper liquid phase sintering effect for the as-mixed powders. Amorphous phase conversion to B2 crystallites seems to be less abrupt than the sudden exothermic Ni/Ti combustion

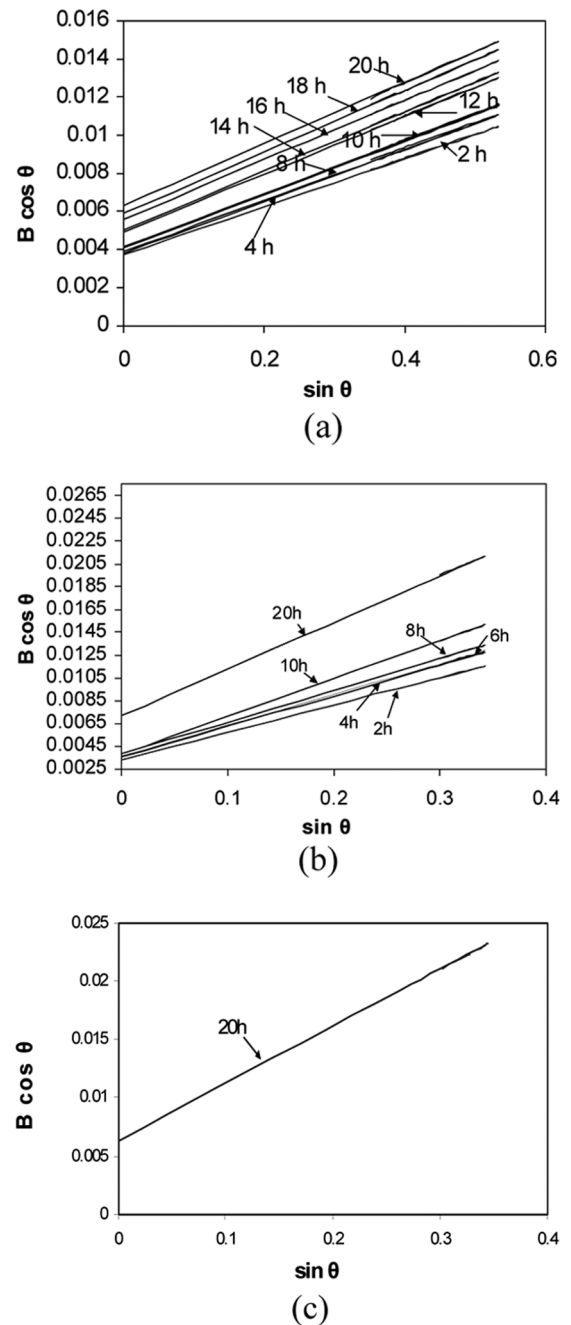


FIGURE 4.—Effect of milling time on Williamson–Hall plot [24] of Ti powders milled at (a) 350rpm characterized by Co- K_{α} , (b) 600 rpm characterized by Cu- K_{α} , and (c) 20 hours milled at 750rpm characterized by Cu- K_{α} .

synthesis process. Evolution of heat would, therefore, be slower with the as-mixed powders than required for partial melting of the Ni/Ti contacting areas within the sample. Liquid phase sintering is thus less feasible with the samples produced from milled powders.

Figure 12 shows that the porosity of the milled/sintered specimens is greater than that of the unmilled ones. Effects of the compaction pressure, sintering time and sintering temperature on pore percentage of the mixed, milled and sintered specimens are shown in Fig. 13. Although the

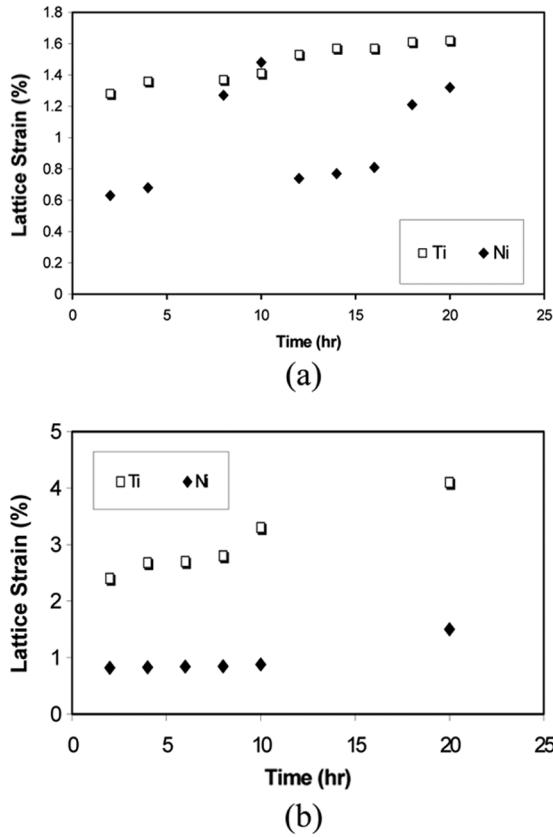


FIGURE 5.—Effect of the milling time on Ti and Ni lattice strain: (a) Co-Kα, 350rpm and (b) Cu-Kα, 600rpm.

starting samples had a low density, different sintering conditions caused a detectable density rise accompanied with porosity reduction as a result of the fixtured sintering treatment.

Fractional porosity, P , defined as the ratio of pore volume to the total volume, can be determined as:

$$P = \left(1 - \frac{\rho}{\rho_{th}}\right) \times 100\% \quad (1)$$

where ρ is the density of the porous material and ρ_{th} is the theoretical density of the corresponding bulk material (6.45 g/cm^3 for Ti-50at.% Ni alloy and 6.19 g/cm^3 for a mixed Ti-50 at.% Ni powder). The densities of the green samples were experimentally determined to be 6.3142 , 6.3162 , and 6.3182 g/cm^3 for 400, 500 and 600MPa of compaction pressure. Their corresponding porosities were 33.32%, 33.295%, and 33.275%.

By increasing temperature and time of sintering, the particles join together to decrease the internal surface area of the samples. Figure 13 shows that the porosity of the mixed sintered specimens decreases with the sintering temperature and time. Sintering results, therefore, in slightly denser samples. For specimens milled for 20 hours and then sintered for different durations, porosity decreases with sintering temperature and time.

Initial collisions cause the FCC ductile nickel powders to work-harden and flatten when they are cold welded and

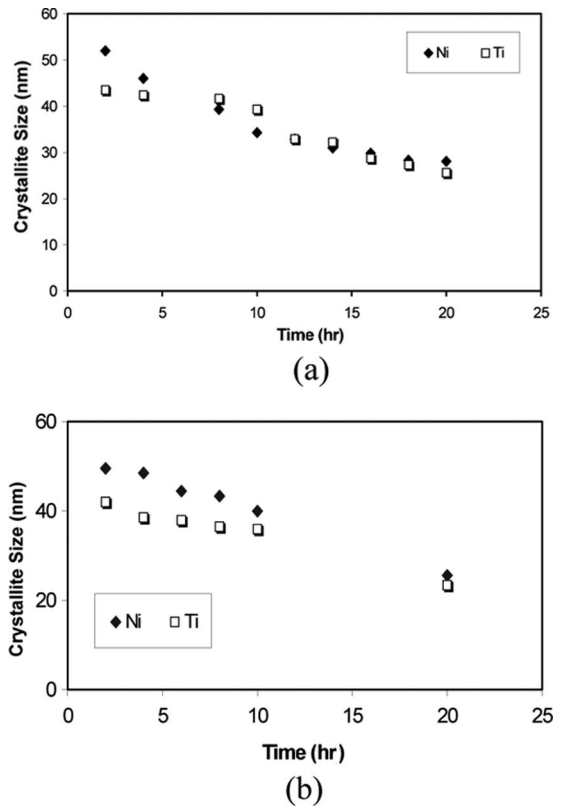


FIGURE 6.—Changes of crystallite size as a function of the milling time: (a) Co-Kα, 350rpm and (b) Cu-Kα, 600rpm.

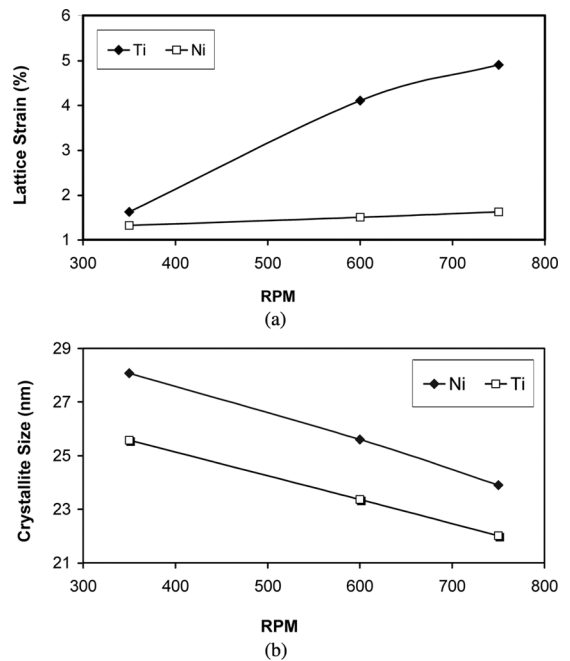


FIGURE 7.—Effect of the milling speed on (a) lattice strain and (b) crystallite size of Ti and Ni after 20 hours of milling.

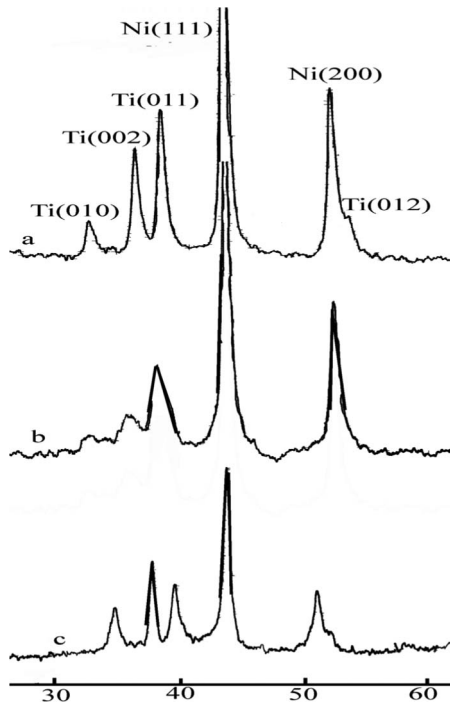


FIGURE 8.—Effect of the speed of milling on the Cu-K α X-ray diffraction spectra of mechanically alloyed powders at: (a) 350rpm, (b) 600rpm, and (c) 750rpm. All samples were milled for 20 hours.

mechanically deformed, heavily. Brittleness of the HCP Ti particles leads, however, to their fracturing. Particles thus flatten, fracture, overlap and produce atomically fresh metallic interfaces. This results in intimate contact which causes the formation of a layered structure.

Further milling results in deformation and cold welding of the layered particles. A refined microstructure is hence obtained. The lamellar spacing of the agglomerated particles is thus reduced. Increasing MA time increases the hardness and results in fracturing of the particles. Agglomerated powders break into smaller aggregates. Long milling times result in an inter-diffusion process that occurs at the fresh surfaces of the intimate powder layers causing the formation of the desirable NiTi phase [33].

Because of the lower melting temperature, the surfaces of the nickel particles may locally melt during the sintering process. Required latent heat may partially be produced by metal-metal pseudo-combustion reaction. A purer metallic interface provides a more active reactant. Higher titanium content can, for example, result in a larger liquefied layer. When this liquid solidifies, shrinkage pores will appear. An increase in porosity can thus be observed.

With mechanically alloyed powders, eventual density of the samples is lower. This is due to the lower reaction speeds with mechanically alloyed small aggregates. The final density of the samples increases with prior-to-sintering compaction pressure. Elimination of the spaces between the particles due to compaction pressure results in lowering of the pore percentages, no matter what initial stage is used to produce the mixture.

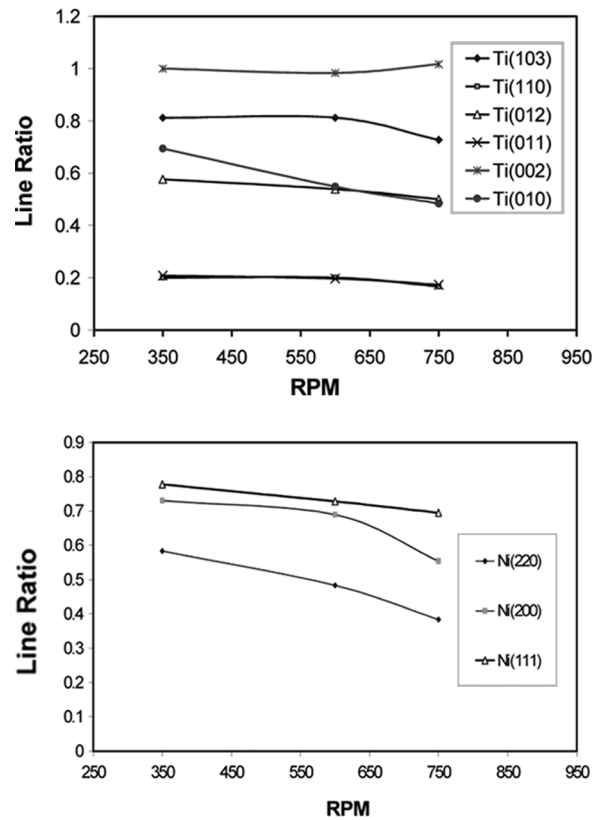


FIGURE 9.—Effect of the speed of milling on the Cu-K α X-ray line ratios of Ti and Ni for different crystallographic planes. All samples have been milled for 20 hours.

Figure 13 shows that the as-mixed samples are less porous than the mechanically alloyed ones. Porosity of both samples reduces, however, as a result of the liquid phase sintering process. Effect of milling on porosity of

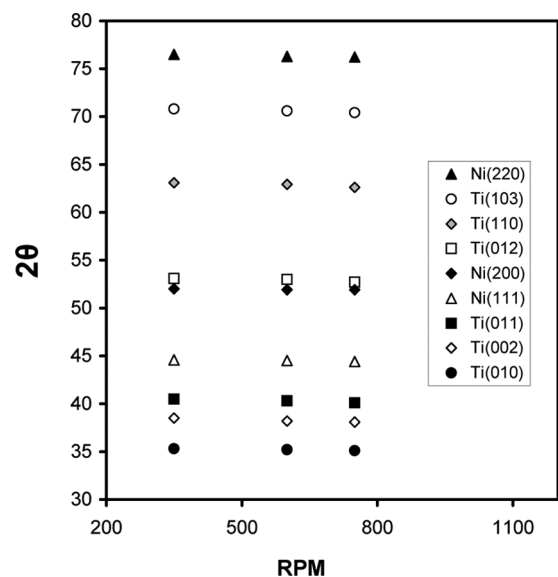


FIGURE 10.—Effect of the speed of milling on the Cu-K α diffraction angles of Ni and Ti.

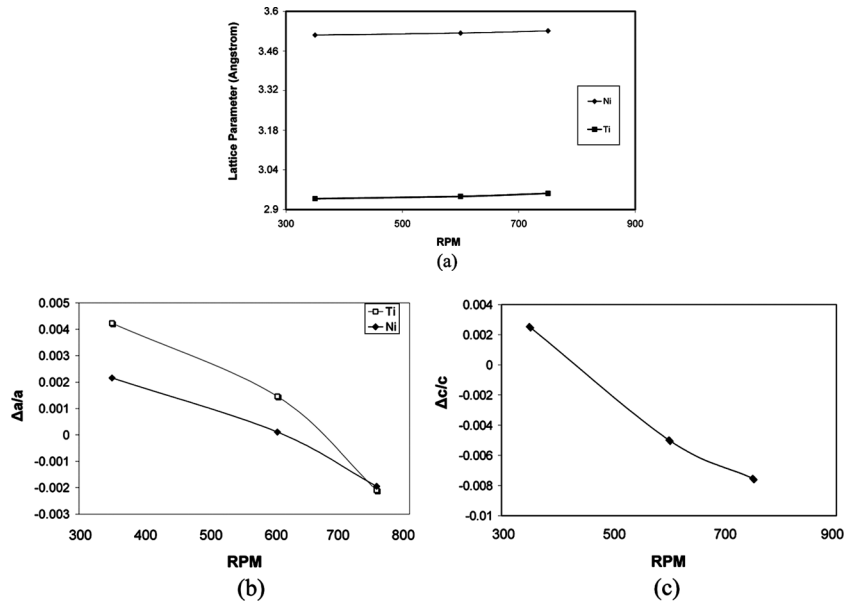


FIGURE 11.—Effect of the speed of milling on (a) the lattice parameter of nickel and titanium crystals, (b) fractional change of lattice parameter a , and (c) fractional change of lattice parameter c .

the samples is inferable from morphologies demonstrated in Fig. 12. It is seen that the porosity of a milled sample is greater than one which is not milled.

Figure 12 illustrates the effect of the milling process on morphology of the sintered samples. The samples shown in parts (a) and (c) of Fig. 12 are made of the as-mixed powders. They subsequently were pressed at 400 MPa and sintered for 4 hr at 1000°C. The other samples were made of the milled powders by the same procedure. These results

are shown in parts (b) and (d) of Figure 12. It is seen that the amount of B19' monoclinic martensitic phase is greater than the amount of the cubic B2 phase. The lower reaction speeds associated with the mechanically alloyed samples result in lower heat evolution during sintering and less NiTi phase formation. Higher austenite–martensite transformation temperatures in the mechanically alloyed samples may be the other reason for this process [33].

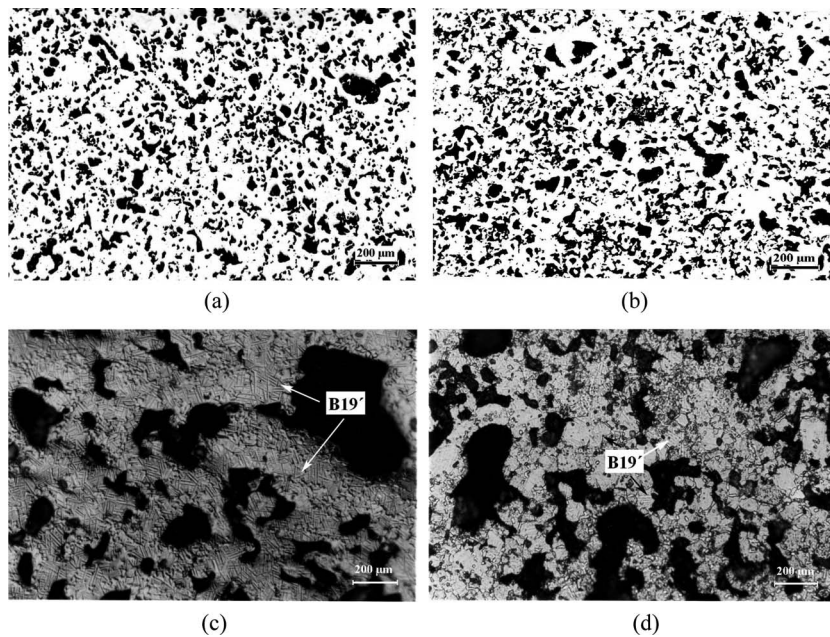


FIGURE 12.—Metallographic pictures of the specimens (a) mixed, pressed and sintered, (b) milled, pressed and sintered, (c) mixed, pressed, sintered and etched, and (d) milled, pressed, sintered and etched.

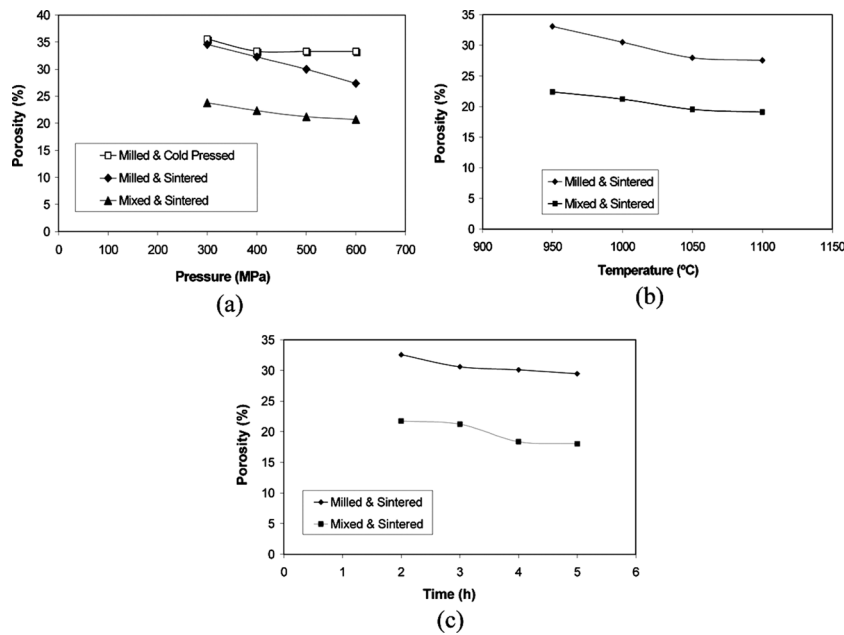


FIGURE 13.—Effect of (a) the compaction pressure, (b) the sintering temperature, and (c) the milling time on the porosity of the mixed, milled and sintered specimens.

PRACTICAL APPLICATIONS

Nanocrystalline porous NiTi material is of great interest from both fundamental and applied research vision. Research and development emphasizes on scientific diversities in generation of materials with controlled microstructural behavior. Nanograined NiTi microtubes have recently been used to make medical devices such as stents designed for less invasive operations. Bulk-sample porosity increase helps osteointegration [5].

Any improvement in practical procedure for production of highly surfaced permanent NiTi implants can increase the success rate and reduce the healing time after a surgical operation [6]. High flexibility, large recoverable deformation, good fatigue life and outstanding superelastic behavior at or around the body temperature allow size reduction of critical medical devices made of nanograined polycrystalline NiTi material [7].

Synthesis, characterization, and processing of nanostructures are part of emerging nanotechnology. High-energy milling is a new way to produce nanocrystalline advanced NiTi material. This process consists of high-energy grinding of a powder mixture for producing amorphous–crystalline composite material [30]. Lowering the amount of the released heat can shift the explosive mode of the combustion process during sintering of the mechanically alloyed samples towards a gradually progressive reaction.

Low-temperature chemical reactions are induced to powder mixtures requiring much higher heat potentials to synthesize at ordinary conditions. It is expected that milling causes particle size reduction, constituent homogenization and particle shape change [31, 32]. Nanometer-scale component interactions are performed at atomically pure planes during high-energy milling. This paper contributes to the mechanical alloying–sintering processes influencing

on porosity percentage and crystallite size of the NiTi semifinished samples. Important properties such as biocompatibility, corrosion resistance and osteointegration seems therefore to be controllable with milling speed, milling time, compression pressure, sintering temperature, and sintering times used during production procedure of the SMA/superelastic samples.

CONCLUSION

NiTi shape-memory alloys can be produced from both elemental and mechanically alloyed aggregate compacts. XRD spectra of the powder mixtures milled for different durations show that the mechanically alloyed NiTi lattice strain increases while the size of the nanocrystallites decreases with the milling time and the rotational speed of the milling apparatus.

Fractured clean surfaces formed during mechanical alloying facilitated the interdiffusion of titanium into nickel. Partial amorphization with crystallization was observed in the NiTi-sintered samples. Vacuum sintering resulted in formation of porous NiTi from as-mixed and 20-hr-milled Ni/Ti powders. Increasing the compaction pressure decreased the porosity of both the as-mixed and the milled samples sintered inside a fixture. This was apparently due to the elimination of the spaces between the powder particles. Shrinkage pore formation due to liquid-phase sintering (LSP) caused porosity enhancement.

The most porous NiTi alloy was obtained by 400MPa pressure, 20-hr milling and 4-hr fixtured sintering at 1050°C. Density of the as-milled compacts increased with the sintering time and temperature. Their porosity decreased with the sintering time and temperature. This seemed to be due to lower internal surface area of the powders when both mechanical and thermal energies associated with the

combined MA/sintering processes could be applied to the samples.

ACKNOWLEDGMENT

The authors wish to thank Mr. A. Selahi for his help in running MA tests and Mr. S.A. Farzadfar for helping in metallographic study of the NiTi samples.

REFERENCES

- Yuan, B.; Chung, C.Y.; Zhu, M. Microstructure and martensitic transformation behavior of porous NiTi shape-memory alloy prepared by hot isostatic pressing processing. *Mater. Sci. Eng. A* **2004**, *382*, 181–187.
- Zhu, S.L.; Yang, X.J.; Hu, F.; Deng, S.H.; Cui, Z.D. Processing of porous TiNi shape-memory alloy from elemental powders by Ar-sintering. *Materials Letters* **2004**, *58*, 2369–2373.
- Puleo, D.A.; Nanci, A. Understanding and controlling the bone-implant interface. *Biomaterials* **1999**, *20*, 2311–2321.
- Li, Y.H.; Rao, G.B.; Rong, L.J.; Li, Y.Y.; Ke, W. Effect of pores on corrosion characteristics of porous NiTi alloy in simulated body fluid. *Materials Science and Engineering A* **2003**, *363*, 356–359.
- Kujala, S.; Ryhanen, J.; Danilov, A.; Tuukkanen, J. Effect of porosity on osteointegration and bone ingrowth of a weight-bearing nickel-titanium bone graft substitute. *Biomaterials* **2003**, *24*, 4691–4697.
- Li, Z.Q.; Sun, Q.P. The initiation and growth of macroscopic martensite band in nano-grained NiTi microtube under tension. *International Journal of Plasticity* **2002**, *18*, 1481–1498.
- Ni, W.; Cheng, Y.T.; Grummon, D.S. Microscopic shape memory and superelastic effects under complex loading conditions. *Surface and Coatings Technology* **2004**, *177*–178, 512–517.
- Saito, S.; Wachi, T.; Hanada, S. New fabrication process of TiNi shape-memory wire. *Materials Science and Engineering A: Structural Materials, Properties, Microstructure and Processing* **1993**, *A 161*, 91–96.
- McNeese, M.D.; Lagoudas, D.C.; Pollock, T.C. Processing of TiNi from elemental powders by hot isostatic pressing. *Mater. Sci. Eng.* **2000**, *A 280*, 334–348.
- Zhang, X.; Sehitoglu, H. Crystallography of the B2→R→B19 phase transformations in NiTi. *Materials Science and Engineering* **2004**, *A 374*, 292–302.
- Otsuka, K.; Ren, X. Physical metallurgy of Ti–Ni-based shape-memory alloys. *Progress in Materials Science* **2005**, *50*, 511–678.
- Elliott, R.S.; Shaw, J.A.; Triantafyllidis, N. Stability of pressure-dependent, thermally-induced displacive transformations in bi-atomic crystals. *International Journal of Solids and Structures* **2002**, *39*, 3845–3856.
- Nemat-Nasser, S.; Su, Y.; Guo, W.G.; Isaacs, J. Experimental characterization and micromechanical modeling of superelastic response of a porous NiTi shape-memory alloy. *Journal of the Mechanics and Physics of Solids* **2005**, *53* (10), 2320–2346.
- Sun, Q.P.; Li, Z.Q. Phase transformation in superelastic NiTi polycrystalline micro-tubes under tension and torsion—from localization to homogeneous deformation. *International Journal of Solids and Structures* **2002**, *39*, 3797–3809.
- Raz, S.B.; Sadrnezhad, S.K. Effects of VIM frequency on chemical composition, homogeneity and microstructure of NiTi shape memory alloy. *Materials Science and Technology* **2004**, *20* (5), 593–598.
- Sadrnezhaad, S.K.; Raz, S.B. Interaction between refractory crucible materials and the melted NiTi shape-memory alloy. *Metallurgical and Materials Transactions B* **2005**, *36B* (3), 395–403.
- Sadrnezhaad, K.; Mashhadi, F.; Sharghi, R. Heat treatment of Ni-Ti alloy for improvement of shape memory effect. *Materials and Manufacturing Processes* **1997**, *12* (1), 107–115.
- Watanabe, S.; Kawata, K.; Kokie, T.; Suda, T.; Ohnuki, S.; Takahashi, H.; Matsukawa, Y.; Kiritani, M. Non-equilibrium local phase formation by high-speed deformation in NiTi. *Materials Science and Engineering* **2003**, *A350*, 145–149.
- Raz, S.B.; Sadrnezhad, S.K. Ingredient losses during melting binary Ni–Ti shape memory alloys. *Journal of Materials Science and Technology* **2005**, *21* (4), 484–488.
- Yeh, C.L.; Sung, W.Y. Synthesis of NiTi intermetallics by self-propagating combustion. *Journal of Alloys and Compounds* **2004**, *376*, 79–88.
- Yuan, B.; Chung, C.Y.; Zhu, M. Microstructure and martensitic transformation behavior of porous NiTi shape memory alloy prepared by hot isostatic pressing processing. *Materials Science and Engineering* **2004**, *A 382*, 181–187.
- Krone, L.; Schuller, E.; Bram, M.; Hamed, O.; Buchkremer, H.P.; Stover, D. Mechanical behavior of NiTi parts prepared by powder metallurgical methods. *Materials Science and Engineering* **2004**, *A 378*, 185–190.
- Bram, M.; Ahmad-Khanlu, A.; Heckmann, A.; Fuchs, B.; Buchkremer, H.P.; Stover, D. Powder metallurgical fabrication processes for NiTi shape-memory alloy parts. *Materials Science and Engineering* **2002**, *A 377*, 254–263.
- Green, S.M.; Grant, D.M.; Kelly, N.R. Powder metallurgical processing of Ni–Ti shape-memory alloy. *Powder Metallurgy* **1997**, *40*, 43–47.
- Li, B.Y.; Rong, L.J.; Li, Y.Y.; Gjunter, V.E. Recent development in producing porous Ni–Ti shape-memory alloys. *Intermetallics* **2000**, *8* (8), 881–884.
- Sadrnezhaad, S.K.; Lashkari, O. Property change during fixtured sintering of NiTi shape-memory alloy. *Materials and Manufacturing Processes* **2005**, *21*, 87–96.
- Fu, Y.; Shearwood, C. Characterization of nanocrystalline TiNi powder. *Scripta Materialia* **2004**, *50*, 319–323.
- Xu, X.; Thadhani, N. Shock synthesis and characterization of nanostructured nitinol alloy. *Materials Science and Engineering* **2004**, *A 384*, 194–201.
- Bertheville, B.; Bidaux, J.E. Alternative powder metallurgical processing of Ti-rich NiTi shape-memory alloys. *Scripta Materialia* **2005**, *52*, 507–512.
- Sadrnezhaad, S.K.; Selahi, A.R. Effect of mechanical alloying and sintering on Ni–Ti powders. *Materials and Manufacturing Processes* **2004**, *19* (3), 475–486.
- Suryanarayana, C. Mechanical alloying and milling. *Progress in Materials Science* **2001**, *46*, 1–184.
- Maziarz, W.; Dutkiewicz, J.; Humbeeck, J.V.; Czeppe, T. Mechanically alloyed and hot-pressed Ni-49.7 Ti alloy showing martensitic transformation. *Materials Science and Engineering* **2004**, *A 375–377*, 844–848.
- Schuller, E.; Bram, M.; Buchkremer, H.P.; Stover, D. Phase transformation temperatures for NiTi alloys prepared by powder metallurgical processes. *Materials Science and Engineering* **2004**, *A 378*, 165–169.